JOURNAL OF GUIDANCE, CONTROL, AND DYNAMICS
Vol. 47, No. 7, July 2024

Engineering Notes

New Angle-Only Observability Criteria for Spaceborne Optimal Evasive Maneuvers Under Perturbations

Yazan Chihabi* and Steve Ulrich†
Carleton University, Ottawa, Ontario K1S 5B6, Canada

https://doi.org/10.2514/1.G008028

I. Introduction

OVER the last few decades, organizations around the world have invested in various civilian and military space capabilities. This is driven by the increasing number of objects of interest, including resident space objects (RSOs), which encompass all near-Earth objects such as debris, spacecraft, and comets and asteroids [1]. Because space is becoming increasingly congested, contested, and competitive, another area that has recently attracted a lot of attention is space situational awareness (SSA), which involves detecting, tracking, identifying, and characterizing RSOs. One of the main objectives of SSA activities is therefore to react to potential threats posed by noncooperative RSOs against space assets. As such, SSA represents a critical capability to enable safe operations in the space domain.

One of the major threats that face space assets is interference by noncooperative RSOs, in the form of unauthorized attempts to perform rendezvous and proximity operations (RPO). It is therefore critical to develop spaceborne guidance and control capabilities to perform orbital evasive maneuvers against such treats. To make those orbital evasive maneuvers capable of reacting autonomously and in real time to unexpected events while on orbit, it is important that they rely on computationally simple guidance and control methodologies. Furthermore, the guidance and control actions must be optimal to ensure that the evasive maneuvers 1) maximize the distance between the space asset to be protected (the evader) and the noncooperative RSO (the pursuer), at the end of the maneuver, while 2) maximizing the pursuer navigation errors. In a scenario where the pursuer RSO can actively sense the motion of the evader through angle-only navigation, it is indeed important to perform evasive maneuvers in a way that induces errors in the pursuer navigation system, thereby reducing the observability of the evasive maneuvers.

The use of angles-only navigation for orbital rendezvous and docking, spacecraft formation flying, and other relative motion applications has been demonstrated by several space missions with increasingly demanding relative navigation requirements that must be achieved autonomously using limited onboard resources [2]. Angle-only relative navigation using a single camera (monocular vision) sensor provides an inherently passive, robust, and high-dynamic range capability due to their low cost, low power consumption, and small size as compared with other systems such as lidar and radar [3,4].

The idea behind solving optimal strategies for multi-agent pursuit-evasion scenarios was first proposed by Isaacs [5]. In this seminal work, the concept of pursuit evasion was first described as a differential game wherein two opposing players aim at either maximizing or minimizing a common objective. The agent who aims at minimizing the objective cost function is considered the pursuer, while the agent which strives at maximizing the same objective cost functional is called the evader. When the strategy of only one agent is deemed to be under control, the differential game simplifies to a single-sided optimization problem. This situation is representative of orbital evasive maneuvers against a noncooperative RSO attempting unauthorized RPO.

Over the years, a few solutions to the optimal evasive problem have been proposed in the context of space debris collision avoidance maneuvers [6–8]. Notably, Kelly and Picciotto [9] proposed an optimal collision avoidance evasive method via a nonlinear optimization approach. Patera and Peterson [10–12] proposed probabilistic optimal evasive strategies. Bombardelli [13] obtained an optimal maneuver method to numerically maximize the miss distance at the predicted collision point. More recently, genetic-algorithm-based approaches were developed by Lee et al. [14] and Kim et al. [15] to solve for evasive maneuvers that optimize fuel consumption. More recently, de Jesus and de Sousa [16] investigated the existence of symmetry in determining the initial conditions of collisions among objects. One major limitation of existing optimal orbital evasive approaches described previously is that they were developed in the context of passive pursuers such as space debris. However, in most operational scenarios, the pursuer is likely to be an active noncooperative RSO capable of sensing and tracking the motion of the evading space asset, through vision-based sensors and thrusters, respectively. Therefore, these solutions are not applicable in an evasive scenario against a pursuer that actively senses, corrects, and/or maintains its own trajectory with respect to the evader.

The first active orbital pursuer–evader problem was studied by Wong [17], who solved the problem from the pursuer perspective for the interception of a maneuverable spacecraft while assuming planar two-body Keplerian motion. Anderson [18] developed a near-optimal feedback control law that effectively allows a pursuer to rendezvous with an active target spacecraft using a modified first-order differential dynamic programming algorithm. Burk and Widhalm [19] developed optimal evasive-maneuver strategies using impulsive and continuous control maneuvers. Wang et al. [20] developed a solution to the pursuer–evader problem based differential game control theory for angle-only navigation based on monocular and binocular vision. Moreover, the formulation is based on Hill's equations of motion and is therefore only optimal for short separation distances and circular orbits. An analytical coplanar orbital evasion strategy is proposed by Yu et al. [21] by considering the variation of relative space geometry and angle-only measurements to find optimal evasive maneuvers. Specifically, the solution uses a genetic algorithm to formulate an analytical solution to the optimal evasive maneuver problem in a pursuer–evader scenario. However, the solution is only applicable to small separation distances (approximately 100 km).

The previously published solutions to the orbital evasion problem rely on simplified representations of the relative motion dynamics based on Hill–Clohessy–Wiltshire (HCW) model [22] that assumes a circular reference orbit. As a result, those solutions to the cost function are not truly optimal due to the simplifications made to the dynamical model used within the cost function. Furthermore, in most of the past methodologies for orbit evasion, the focus was on nonmaneuvering RSOs rather than on active pursuers. For the cases

Presented as Paper AAS 23-110 at the 33rd AAS/AIAA Space Flight Mechanics Meeting, Austin, TX, January 15–19, 2023; received 23 October 2023; accepted for publication 2 April 2024; published online 10 May 2024.

*Ph.D. Candidate, Department of Mechanical and Aerospace Engineering, 1125 Colonel By Drive; yazanchihabi@cmail.carleton.ca. Student Member AIAA (Corresponding Author).

†Associate Professor, Department of Mechanical and Aerospace Engineering, 1125 Colonel By Drive. Associate Fellow AIAA.

where an active pursuer is considered, the dynamical model used is only applicable to small separation distances and coplanar orbits and therefore would not provide an optimal solution that renders the pursuer angle-only navigation system unobservable. In this context, the main objective of this work is to develop innovative orbital evasive maneuvers in response to an active, yet noncooperative, RSO attempting unauthorized RPO. Autonomous and real-time capabilities are ensured through the development of computationally simple spaceborne guidance and control algorithms. Optimal performance of the evasive maneuvers, in terms of maximizing evader–pursuer separation distances and therefore ensuring unobservability of the pursuer's relative navigation system, is guaranteed through the use of a highly accurate relative motion dynamical model that relies of perturbed state-transition matrices recently developed by Chihabi and Ulrich [23–25]. This dynamical formulation was recently used for spacecraft formation flying to develop a two-point guidance law that determines the optimal trajectory in a desired time interval [26,27]. As such, this work extends the optimal guidance technique in Ref. [27] to develop an algorithm that determines an evasive trajectory and control maneuvers that renders the pursuer angle-only navigation system unobservable. This is done by integrating previously established analyses of vision-based-only relative motion observability criteria within the optimal guidance algorithm to maximize the pursuer navigation errors [28–33]. Furthermore, the use of the highly accurate dynamical model with optimal control theory ensures that the evader spacecraft performs optimized and fuel-efficient evasive maneuvers.

II. Preliminaries

This section presents the preliminaries required to formulate the optimal evasive maneuver strategies. Specifically, Woffinden and Geller's [2] observability criteria are briefly described, along with spacecraft relative dynamics based on relative orbital elements (ROEs) [23–25] and finally optimal control theory (see [34] pp. 120–124), which will be combined to derive optimal evasive maneuvers in a pursuer–evader scenario such that the evader renders the pursuer's onboard angle-only navigation system unobservable.

A. Angle-Only Observability Criteria

This subsection reviews the observablility criteria formulated by Woffinden and Geller [2] modified for application with a pursuer–evader scenario. The development of the observability criteria assumes that the pursuer is in a circular reference orbit with the evader having a linear relative motion profile according to the following state-space model such that the HCW model [22] can be used to model the relative motion, for which the resulting state-space formulation is given by

$$\dot{\boldsymbol{x}} = \boldsymbol{A}\boldsymbol{x} + \boldsymbol{B}\boldsymbol{u} \tag{1}$$

with

$$\boldsymbol{A} = \begin{bmatrix} 0 & 0 & 0 & 1 & 0 & 0 \\ 0 & 0 & 0 & 0 & 1 & 0 \\ 0 & 0 & 0 & 0 & 0 & 1 \\ 3n^2 & 0 & 0 & 0 & 2n & 0 \\ 0 & 0 & 0 & -2n & 0 & 0 \\ 0 & 0 & -n^2 & 0 & 0 & 0 \end{bmatrix} \quad \boldsymbol{B} = \begin{bmatrix} 0 & 0 & 0 \\ 0 & 0 & 0 \\ 0 & 0 & 0 \\ 1 & 0 & 0 \\ 0 & 1 & 0 \\ 0 & 0 & 1 \end{bmatrix}$$

$$\boldsymbol{x} = \begin{bmatrix} \boldsymbol{\rho}^T & \dot{\boldsymbol{\rho}}^T \end{bmatrix}^T = \begin{bmatrix} x & y & z & \dot{x} & \dot{y} & \dot{z} \end{bmatrix}^T \quad \boldsymbol{u} = \begin{bmatrix} u_x & u_y & u_z \end{bmatrix}^T$$

where $\boldsymbol{\rho}$ denotes denotes the position of the evader with respect to the pursuer with components $[\,x \quad y \quad z\,]^T$ in the radial, along-track, and cross-track directions of the local-vertical–local-horizontal (LVLH) reference frame, $\boldsymbol{u}$ denotes the control acceleration of the evader spacecraft, and n denotes the mean orbital motion of the pursuer spacecraft.

Based on linear time-invariant system dynamics, the solution of the state-space model can be determined as

$$\boldsymbol{x}(\tau) = \boldsymbol{\Phi}(\tau, \tau_0)\boldsymbol{x}(\tau_0) + \int_{\tau_0}^{\tau} \boldsymbol{\Phi}(\tau, \mu)\boldsymbol{B}\boldsymbol{u}(\mu)\,\mathrm{d}\mu \tag{2}$$

where the state-transition matrix denoted by $\boldsymbol{\Phi}(\tau, \tau_0)$ is given by

$$\boldsymbol{\Phi}(\tau, \tau_0) = \boldsymbol{I} + \boldsymbol{A}\Delta\tau + \frac{\boldsymbol{A}^2\Delta\tau^2}{2!} \tag{3}$$

where $\boldsymbol{I}$ denotes the identity matrix and $\Delta\tau = \tau - \tau_0$. Alternatively, Eq. (2) can be expanded as

$$\begin{bmatrix} \boldsymbol{\rho}(\tau) \\ \dot{\boldsymbol{\rho}}(\tau) \end{bmatrix} = \begin{bmatrix} \boldsymbol{\Phi}_{\rho\rho} & \boldsymbol{\Phi}_{\rho\dot{\rho}} \\ \boldsymbol{\Phi}_{\dot{\rho}\dot{\rho}} & \boldsymbol{\Phi}_{\dot{\rho}\rho} \end{bmatrix} \begin{bmatrix} \boldsymbol{\rho}_0 \\ \dot{\boldsymbol{\rho}}_0 \end{bmatrix} + \int_{\tau_0}^{\tau} \begin{bmatrix} \boldsymbol{\Phi}_{\rho\rho}(\tau, \mu) & \boldsymbol{\Phi}_{\rho\dot{\rho}}(\tau, \mu) \\ \boldsymbol{\Phi}_{\dot{\rho}\dot{\rho}}(\tau, \mu) & \boldsymbol{\Phi}_{\dot{\rho}\rho}(\tau, \mu) \end{bmatrix} \begin{bmatrix} \boldsymbol{0} \\ \boldsymbol{I} \end{bmatrix} \boldsymbol{u}(\mu)\,\mathrm{d}\mu \tag{4}$$

The angle measurements can be rewritten as a LOS unit vector measurement $\boldsymbol{i}_m$ equivalent to the unit vector of the position of the evader with respect to the pursuer based on the description in Fig. 1, that is,

$$\begin{aligned} \boldsymbol{i}_m(\tau) &= \begin{bmatrix} \cos(\alpha_m(\tau))\cos(\beta_m(\tau)) & \sin(\alpha_m(\tau))\cos(\beta_m(\tau)) & \sin(\beta_m(\tau)) \end{bmatrix}^T \\ &= \frac{\boldsymbol{\rho}(\tau)}{||\boldsymbol{\rho}(\tau)||} \end{aligned} \tag{5}$$

where α_m and β_m denote the measured azimuth and elevation angles, respectively. Solving for $\boldsymbol{\rho}(\tau)$ from Eq. (4) and substituting into Eq. (5) results in

$$\boldsymbol{i}_m(\tau) = \frac{\boldsymbol{\Phi}_{\rho\rho}\boldsymbol{\rho}_0 + \boldsymbol{\Phi}_{\rho\dot{\rho}}\dot{\boldsymbol{\rho}}_0 + \int_{\tau_0}^{\tau} \boldsymbol{\Phi}_{\rho\dot{\rho}}(\tau, \mu)\boldsymbol{u}(\mu)\,\mathrm{d}\mu}{\left|\left|\boldsymbol{\Phi}_{\rho\rho}\boldsymbol{\rho}_0 + \boldsymbol{\Phi}_{\rho\dot{\rho}}\dot{\boldsymbol{\rho}}_0 + \int_{\tau_0}^{\tau} \boldsymbol{\Phi}_{\rho\dot{\rho}}(\tau, \mu)\boldsymbol{u}(\mu)\,\mathrm{d}\mu\right|\right|} \tag{6}$$

Whenever control input is applied along the line-of-sight (LOS) direction (along $\boldsymbol{\rho}$), the equality (7) is satisfied

$$\int_{\tau_0}^{\tau} \boldsymbol{\Phi}_{\rho\dot{\rho}}(\tau, \mu)\boldsymbol{u}(\mu)\,\mathrm{d}\mu = \eta(\tau)\left[\boldsymbol{\Phi}_{\rho\rho}\boldsymbol{\rho}_0 + \boldsymbol{\Phi}_{\rho\dot{\rho}}\dot{\boldsymbol{\rho}}_0\right] \tag{7}$$

and substituting this equality into Eq. (6) results in

$$\begin{aligned} \boldsymbol{i}_m(\tau) &= \frac{\boldsymbol{\Phi}_{\rho\rho}\boldsymbol{\rho}_0 + \boldsymbol{\Phi}_{\rho\dot{\rho}}\dot{\boldsymbol{\rho}}_0 + \eta(\tau)[\boldsymbol{\Phi}_{\rho\rho}\boldsymbol{\rho}_0 + \boldsymbol{\Phi}_{\rho\dot{\rho}}\dot{\boldsymbol{\rho}}_0]}{\left|\left|\boldsymbol{\Phi}_{\rho\rho}\boldsymbol{\rho}_0 + \boldsymbol{\Phi}_{\rho\dot{\rho}}\dot{\boldsymbol{\rho}}_0 + \eta(\tau)[\boldsymbol{\Phi}_{\rho\rho}\boldsymbol{\rho}_0 + \boldsymbol{\Phi}_{\rho\dot{\rho}}\dot{\boldsymbol{\rho}}_0]\right|\right|} \\ &= \frac{[1 + \eta(\tau)][\boldsymbol{\Phi}_{\rho\rho}\boldsymbol{\rho}_0 + \boldsymbol{\Phi}_{\rho\dot{\rho}}\dot{\boldsymbol{\rho}}_0]}{\left|\left|[1 + \eta(\tau)][\boldsymbol{\Phi}_{\rho\rho}\boldsymbol{\rho}_0 + \boldsymbol{\Phi}_{\rho\dot{\rho}}\dot{\boldsymbol{\rho}}_0]\right|\right|} \end{aligned} \tag{8}$$

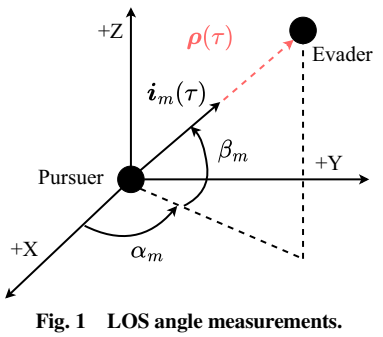

Fig. 1 LOS angle measurements.

where $\eta(\tau)$ is a multiplication factor for the LOS vector that can be either constant or time varying.

As shown in Eq. (8), the LOS measurement profile will not result in any change when $\eta(\tau) > -1$ and therefore will not produce any observability, rendering the measurements unobservable as shown in Fig. 2a. This is due to the fact that the range or scale on the initial conditions cannot be determined. Any maneuvers that act along the LOS vector will result in unobservable measurements, regardless of the scale. Table 1 summarizes the observability criteria.

$$\boldsymbol{\Phi}_{\text{LVLH}} = \begin{bmatrix} \frac{r_p}{a_p} & -a_p\cos\theta_p & 0 & 0 & 0 & \frac{a_p e_p \sin\theta_p}{\sqrt{1-e_p{}^2}} \\ 0 & \frac{r_p \sin\theta_p}{1-e_p{}^2}(2+e_p\cos\theta_p) & 0 & r_p & r_p\cos i_p & \frac{r_p}{(1-e_p{}^2)^{3/2}} \\ 0 & 0 & r_p\sin\theta_p & 0 & -r_p\cos\theta_p\sin\theta_p & 0 \end{bmatrix} \tag{11}$$

B. Spacecraft Relative Dynamics Based on Relative Orbital Elements

Woffinden and Geller's [2] observability criteria are derived based on the HCW model, which is only applicable to circular reference orbits. As such, this subsection provides a brief overview of the ROE-based equations of motion that will be used instead of the HCW model to formulate new ROE-based observability criteria for angle-only navigation which is applicable to arbitrary eccentric orbits [23–25]. A full analysis of the dynamical model, including effects of fourth-order luni-solar third-body perturbations, solar radiation pressure, atmospheric drag, and gravitational field up to the fifth zonal harmonic, can be found in Refs. [23,25].

1. *Linearized Equations of Relative Motion Using Relative Orbital Elements*

The nonlinear equations of motion formulated by Gurfil and Kholshevnikov [35,36] provide a method of calculating the relative motion of two spacecraft in the LVLH reference frame using each spacecraft's orbital elements. However, orbital elements cannot be determined from Cartesian coordinates using these equations. In turn, these equations cannot be used to determine ROE using a set of desired Cartesian coordinates. Schaub and Junkins derived the linearized equations of motion using a first-order approximation, which is presented in state-space form as [37]

$$\boldsymbol{\rho}(\tau) = [\,x \quad y \quad z\,]^T = \boldsymbol{\Phi}_{\text{LVLH}}\Delta\boldsymbol{\alpha} \tag{9}$$

where

$$\boldsymbol{\alpha} = [\,a \quad e \quad i \quad \omega \quad \Omega \quad M\,]^T \tag{10}$$

where the variables a, e, i, Ω, ω, θ, and M denote the semimajor axis, eccentricity, inclination, right ascension of the ascending node, argument of perigee, true anomaly, and mean anomaly, respectively. The variable $\Delta\boldsymbol{\alpha}$ contains the difference in orbital elements between the evader and the pursuer spacecraft such that $\Delta\boldsymbol{\alpha} = \boldsymbol{\alpha}_e - \boldsymbol{\alpha}_p$, where the subscripts e and p denote the evader and pursuer, respectively. The pursuer's distance, speed, true anomaly, and rate (r_p, $\dot{r}_p$, θ_p, and $\dot{\theta}_p$) are given in Ref. [38].

2. *Unforced Relative Orbital Elements Dynamical Model*

This subsection briefly describes the unforced relative dynamics for two spacecraft in terms of orbital elements. The orbital dynamics are defined as

$$\dot{\boldsymbol{\alpha}}^a = \begin{bmatrix} \dot{a} & \dot{e} & \dot{i} & \dot{\omega} & \dot{\Omega} & \dot{M} & \dot{B}^{\text{SRP}} & \dot{B}^{\text{drag}} \end{bmatrix}^T = \boldsymbol{f}(\boldsymbol{\alpha}^a) \tag{12}$$

where $\boldsymbol{\alpha}$ is augmented to include ballistic coefficients of solar radiation pressure (SRP) and atmospheric drag, denoted by B^{SRP} and $\dot{B}^{\text{drag}}$, such that $\boldsymbol{\alpha}^a = [\,a \quad e \quad i \quad \omega \quad \Omega \quad M \quad B^{\text{SRP}} \quad B^{\text{drag}}\,]^T$. The ballistic coefficients are given by

$$B^{\text{SRP}} = \frac{C_r A}{m} \qquad B^{\text{drag}} = \frac{C_D A}{m}$$

where C_r and C_D denote the coefficients of reflectivity and atmospheric drag, respectively; A represents the exposed area in m^2; and m denotes the mass of the spacecraft. The resulting dynamics is the combination of Keplerian and total perturbing effects considered represented by

$$\boldsymbol{f}(\boldsymbol{\alpha}^a) = \boldsymbol{f}_{\text{kep}}(\boldsymbol{\alpha}^a) + \sum \boldsymbol{f}_{\text{per}}(\boldsymbol{\alpha}^a) \tag{13}$$

where

$$\boldsymbol{f}_{\text{kep}}(\boldsymbol{\alpha}^a) = [\,0 \quad 0 \quad 0 \quad 0 \quad 0 \quad n \quad 0 \quad 0\,]^T \tag{14}$$

$$\boldsymbol{f}_{\text{per}}(\boldsymbol{\alpha}^a) = \begin{bmatrix} \dot{a}_{\text{per}} & \dot{e}_{\text{per}} & \dot{i}_{\text{per}} & \dot{\omega}_{\text{per}} & \dot{\Omega}_{\text{per}} & \dot{M}_{\text{per}} & 0 & 0 \end{bmatrix}^T \tag{15}$$

where subscript $\{\}_{\text{per}}$ denotes the perturbed terms. The system dynamics can now be expressed in terms of relative orbital elements by taking the Jacobian of Eq. (12) as

$$\Delta\dot{\boldsymbol{\alpha}}^a = \boldsymbol{F}(\tau)\Delta\boldsymbol{\alpha}^a \tag{16}$$

where

$$\boldsymbol{F}(\tau) = \left.\frac{\partial \boldsymbol{f}(\boldsymbol{\alpha}^a)}{\partial \boldsymbol{\alpha}^a}\right|_{\boldsymbol{\alpha}=\boldsymbol{\alpha}_p^a} \tag{17}$$

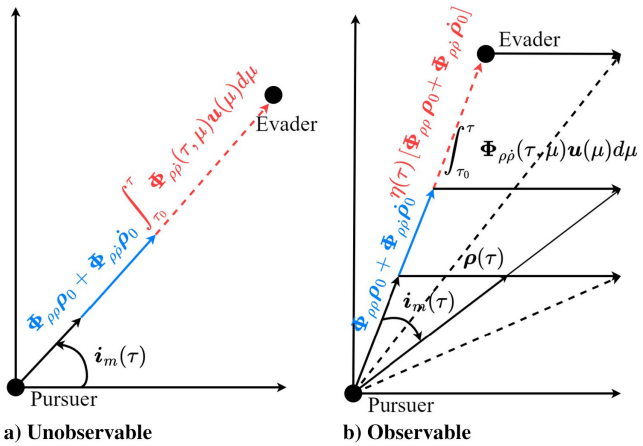

a) Unobservable b) Observable

Fig. 2 Unobservable and observable maneuver profiles.

Table 1 Observability criteria

Observable	$\int_{\tau_0}^{\tau} \boldsymbol{\Phi}_{\rho\dot{\rho}}(\tau,\mu)\boldsymbol{u}(\mu)\,\mathrm{d}\mu \neq \eta(\tau)\left[\boldsymbol{\Phi}_{\rho\rho}\rho_0 + \boldsymbol{\Phi}_{\rho\dot{\rho}}\dot{\rho}_0\right]$	for any $\eta(\tau)$
Observable	$\int_{\tau_0}^{\tau} \boldsymbol{\Phi}_{\rho\dot{\rho}}(\tau,\mu)\boldsymbol{u}(\mu)\,\mathrm{d}\mu = \eta(\tau)\left[\boldsymbol{\Phi}_{\rho\rho}\rho_0 + \boldsymbol{\Phi}_{\rho\dot{\rho}}\dot{\rho}_0\right]$	for $\eta(\tau) < -1$
Unobservable	$\int_{\tau_0}^{\tau} \boldsymbol{\Phi}_{\rho\dot{\rho}}(\tau,\mu)\boldsymbol{u}(\mu)\,\mathrm{d}\mu = \eta(\tau)\left[\boldsymbol{\Phi}_{\rho\rho}\rho_0 + \boldsymbol{\Phi}_{\rho\dot{\rho}}\dot{\rho}_0\right]$	for $\eta(\tau) > -1$

The matrices that make up the Jacobian matrix $\boldsymbol{F}(\tau)$ are given by Chihabi and Ulrich [23,25] and contain the perturbing effects of J_2 luni-solar third-body, atmospheric drag and SRP. The mapping of the augmented orbital elements to the relative position in LVLH reference frame is also augmented as follows:

$$\rho(\tau) \quad = [\,x \quad y \quad z\,]^T = \boldsymbol{\Phi}^a_{\text{LVLH}} \Delta\boldsymbol{\alpha}^a \tag{18}$$

where

$$\boldsymbol{\Phi}^a_{\text{LVLH}} = [\,\boldsymbol{\Phi}_{\text{LVLH}} \quad \boldsymbol{0}_{3\times 2}\,] \tag{19}$$

3. Forced Linear Time-Varying Relative Orbital Elements Dynamical Model

The system dynamics of spacecraft relative motion can be expressed in terms of relative orbital elements and chaser control actuation by adding the newly developed second-order integral form of Gauss's variational equations (GVEs) [39] to the equation presented in Eq. (16) as

$$\Delta\dot{\boldsymbol{\alpha}}^a = \boldsymbol{F}(\tau)\Delta\boldsymbol{\alpha}^a + \boldsymbol{B}(\tau)\boldsymbol{u} \tag{20}$$

where

$$\boldsymbol{B}(\tau) = \boldsymbol{B}'(\tau) + \boldsymbol{B}''(\tau) \tag{21}$$

$$\boldsymbol{B}'(\tau) = \begin{bmatrix} \frac{2\,a^2\,e\,\sin(\theta)}{h} & \frac{p\,\sin(\theta)}{h} & 0 & -\sqrt{\frac{p}{\mu}}\frac{\cos(\theta)}{e} & 0 & -\frac{\eta\,(2\,e\,r - p\,\cos(\theta))}{e\,h} & 0 & 0 \\ \frac{2\,a^2}{h\,r} & \frac{e\,r+\cos(\theta)\,(p+r)}{h} & 0 & \frac{\sin(\theta)\,(p+r)}{e\,h} & 0 & -\frac{\eta\,\sin(\theta)\,(p+r)}{e\,h} & 0 & 0 \\ 0 & 0 & \frac{r\,\cos(\theta+w)}{h} & -\frac{r\,\sin(\theta+w)\,\cos(\mathrm{i})}{h\,\sin(\mathrm{i})} & \frac{r\,\sin(\theta+w)}{h\,\sin(\mathrm{i})} & 0 & 0 & 0 \end{bmatrix}^T \tag{22}$$

$$\boldsymbol{B}''(\tau) = \begin{bmatrix} \boldsymbol{G}_1^T\boldsymbol{u} & \boldsymbol{G}_2^T\boldsymbol{u} & \boldsymbol{G}_3^T\boldsymbol{u} & \boldsymbol{G}_4^T\boldsymbol{u} & \boldsymbol{G}_5^T\boldsymbol{u} & \boldsymbol{G}_6^T\boldsymbol{u} & \boldsymbol{0}_{3\times 2} \end{bmatrix}^T \tag{23}$$

and $\boldsymbol{u} \in \mathbb{R}^3$ is the control acceleration of the evader spacecraft expressed in its own orbital reference frame; the variable h denotes the target's orbital angular momentum, calculated as $h = \sqrt{\mu a(1-e^2)}$; and $\eta = \sqrt{1-e^2}$. The second-order mapping of the control inputs to the rate of change of orbital elements, represented by matrices $\boldsymbol{G}_1$ to $\boldsymbol{G}_6$, are given in [27], and the elements of matrix $\boldsymbol{B}(\tau)$ are evaluated at the target's time-varying orbital elements, using the analytical equations for two-body plus perturbations discussed in the previous section.

C. Optimal Control Theory

Finally, this subsection presents a brief overview of nonlinear optimal control theory as described by Lewis [34], which is used to derive a guidance and control law for optimal evasive maneuvers based on the observability criteria and ROE-based relative dynamics. A nonlinear time-varying dynamical system in state-variable form is given by ([34] pp. 120–124)

$$\dot{\boldsymbol{x}} = f(\boldsymbol{x}, \boldsymbol{u}, \tau) \tag{24}$$

where $\boldsymbol{x}(\tau) \in \mathbb{R}^n$ is an arbitrary state vector and $\boldsymbol{u}(\tau) \in \mathbb{R}^m$ are the time-varying control inputs of the system. The objective of optimal control theory is, in general, to determine control input $\boldsymbol{u}(\tau)$ that minimizes a performance index (PI) or cost function given by

$$J(\tau_0) = \phi(\boldsymbol{x}(\tau_f), \tau_f) + \int_{\tau_0}^{\tau_f} L(\boldsymbol{x}(\tau), \boldsymbol{u}(\tau), \tau)\,\mathrm{d}\tau \tag{25}$$

where $\phi(\boldsymbol{x}(\tau_f), \tau_f)$ is a final state weight function and $L(\boldsymbol{x}(\tau), \boldsymbol{u}(\tau), \tau)$ is an integral weight function that require minimization. In addition to minimizing the previous cost function, the objective of the optimal control problem is to ensure the final state constraint $\Psi \in \mathbb{R}^p$ goes to zero, as

$$\Psi(\boldsymbol{x}(\tau_f), \tau_f) = \boldsymbol{0}_p \tag{26}$$

where p is the order of state constraints.

The solution to the optimal control problem involves the use of Lagrange multipliers to relate the previous optimal control equations. To satisfy the constraints given by Eqs. (24) and (26), the cost function of Eq. (25) is augmented as (see [34] pp. 120–124)

$$J' = \phi(\boldsymbol{x}(\tau_f), \tau_f) + \boldsymbol{\nu}^T\Psi(\boldsymbol{x}(\tau_f), \tau_f) + \int_{\tau_0}^{\tau_f} \left[L(\boldsymbol{x}(\tau), \boldsymbol{u}(\tau), \tau) + \boldsymbol{\lambda}^T(\tau)(f(\boldsymbol{x}, \boldsymbol{u}, \tau) - \dot{\boldsymbol{x}})\right]\mathrm{d}\tau \tag{27}$$

where $\boldsymbol{\lambda}(\tau) \in \mathbb{R}^n$ and $\boldsymbol{\nu} \in \mathbb{R}^p$ are time-varying and constant associated Lagrange multipliers, respectively. This leads to the Hamiltonian function

$$H(\boldsymbol{x}, \boldsymbol{u}, \tau) = L(\boldsymbol{x}(\tau), \boldsymbol{u}(\tau), \tau) + \boldsymbol{\lambda}^T(\tau) f(\boldsymbol{x}, \boldsymbol{u}, \tau) \tag{28}$$

with the well-known Hamilton's equations for the states and costates

$$\dot{\boldsymbol{x}} = \frac{\partial H}{\partial \boldsymbol{\lambda}} = f(\boldsymbol{x}, \boldsymbol{u}, \tau),\ \tau \geq \tau_0 \tag{29}$$

$$-\dot{\boldsymbol{\lambda}} = \frac{\partial H}{\partial \boldsymbol{x}} = \frac{\partial f^T}{\partial \boldsymbol{x}}\boldsymbol{\lambda} + \frac{\partial L}{\partial \boldsymbol{x}},\ \tau \leq \tau_f \tag{30}$$

Equations (29) and (30) must satisfy the following stationary and boundary conditions:

$$\textbf{stationary conditions:} \quad \frac{\partial H}{\partial \boldsymbol{u}} = \frac{\partial f^T}{\partial \boldsymbol{u}}\boldsymbol{\lambda} + \frac{\partial L}{\partial \boldsymbol{u}} = 0 \tag{31}$$

$$\textbf{boundary conditions:} \quad \boldsymbol{x}(\tau_0) = \boldsymbol{x}_0 \tag{32}$$

$$\left(\phi_x + \Psi_x^T\boldsymbol{\nu} - \boldsymbol{\lambda}\right)^T\Big|_{\tau_f} d\boldsymbol{x}(\tau_f) + \left(\phi_p + \Psi_p^T\boldsymbol{\nu} + H\right)^T\Big|_{\tau_f} d\tau_f = 0 \tag{33}$$

where the subscripts x and τ denote the matrix derivatives with respect to the states and time, respectively. These conditions are also known as Euler's equations. The boundary conditions given by Eqs. (32) and (33) are necessary to solve the Hamiltonian system and hence to determine the optimal control that achieves these conditions. In other words, the optimal control $\boldsymbol{u}(\tau)$ is evaluated in terms of the states $\boldsymbol{x}(\tau)$ and costates $\boldsymbol{\lambda}(\tau)$.

III. Optimal Evasive Maneuvers Formulation

In this section, a new optimal guidance and control formulation for computing optimal evasive maneuvers in a pursuer–evader scenario is developed using ROE-based dynamics presented by Eq. (20). In

particular, the development uses optimal control theory in combination with ROE-based dynamics to determine a new set of angle-only observability criteria by modifying Woffinden and Geller's [2] existing criteria. The new formulation determines the optimal path and maneuvers using the pursuer spacecraft's initial conditions and a desired maneuver time while minimizing the control effort.

A. Open-Loop Linear Time-Varying Quadratic Control Law

The development of the evasive maneuver control law is based on the optimal guidance algorithm found in Ref. [27] and is used in the formulation of evasive maneuver. The algorithm begins by selecting a simple quadratic cost function as

$$J(\tau_0) = \phi(\boldsymbol{\alpha}^a(\tau_f), \tau_f) + \boldsymbol{\nu}^T \Psi(\boldsymbol{\alpha}^a(\tau_f), \tau_f) + \int_{\tau_0}^{\tau_f} \frac{1}{2} \boldsymbol{u}^T \boldsymbol{R} \boldsymbol{u} \, \mathrm{d}\tau \quad (34)$$

which results in the Hamiltonian system

$$H = \frac{1}{2} \boldsymbol{u}^T \boldsymbol{R} \boldsymbol{u} + \boldsymbol{\lambda}^T [\boldsymbol{F} \Delta \boldsymbol{\alpha}^a + \boldsymbol{B}(\tau) \boldsymbol{u}] \quad (35)$$

$$\Delta \dot{\boldsymbol{\alpha}}^a = \boldsymbol{F} \Delta \boldsymbol{\alpha}^a + \boldsymbol{B}(\tau) \boldsymbol{u} \quad (36)$$

$$\dot{\boldsymbol{\lambda}} = -\boldsymbol{F}^T \boldsymbol{\lambda} \quad (37)$$

subject to the constraints

$$\phi\big(\boldsymbol{\alpha}^a(\tau_f), \tau_f\big) = \frac{1}{2} \Big[\Delta \boldsymbol{\alpha}^a(\tau_f) - \Delta \boldsymbol{\alpha}_d^a(\tau_f)\Big]^T \Big[\Delta \boldsymbol{\alpha}^a(\tau_f) - \Delta \boldsymbol{\alpha}_d^a(\tau_f)\Big] \quad (38)$$

$$\Psi\big(\boldsymbol{\alpha}^a(\tau_f), \tau_f\big) = \Big[\Delta \boldsymbol{\alpha}^a(\tau_f) - \Delta \boldsymbol{\alpha}_d^a(\tau_f)\Big] = \boldsymbol{0}_8 \quad (39)$$

where $\Delta \boldsymbol{\alpha}_d^a$ is the desired relative orbital elements at the final time τ_f and $\boldsymbol{R}$ is the weight at which the control energy is penalized. The optimal control problem can be further simplified by the fact that the final time is known with $\tau_f = 0$,

$$\big(\phi_{\boldsymbol{\alpha}^a} + \Psi_{\boldsymbol{\alpha}^a}^T \boldsymbol{\nu} - \boldsymbol{\lambda}\big)^T \big|_{\tau_f} d\Delta \boldsymbol{\alpha}^a(\tau_f) = \big(\phi_{\boldsymbol{\alpha}^a} - \boldsymbol{\lambda}\big)^T \big|_{\tau_f} d\Delta \boldsymbol{\alpha}^a(\tau_f) = 0 \quad (40)$$

which implies

$$\boldsymbol{\lambda}(\tau_f) = \phi_{\boldsymbol{\alpha}^a} = \Delta \boldsymbol{\alpha}^a(\tau_f) - \Delta \boldsymbol{\alpha}_d^a(\tau_f) \quad (41)$$

Applying the stationary condition from Eq. (31), the constraint that guarantees minimization of the cost function with respect to the control acceleration needed, to Eq. (36) results in

$$\boldsymbol{u} = -\boldsymbol{R}^{-1} \boldsymbol{B}^T(\tau) \boldsymbol{\lambda}(\tau) \quad (42)$$

This is referred to the open-loop linear time-varying quadratic control law. Substituting the previous equation into Eq. (36) and expressing it in a linear time-varying state-space form gives

$$\begin{bmatrix} \Delta \dot{\boldsymbol{\alpha}}^a \\ \dot{\boldsymbol{\lambda}} \end{bmatrix} = \begin{bmatrix} \boldsymbol{F}(\tau) & -\boldsymbol{B}(\tau) \boldsymbol{R}^{-1} \boldsymbol{B}^T(\tau) \\ \boldsymbol{0}_{8\times 8} & -\boldsymbol{F}(\tau)^T \end{bmatrix} \begin{bmatrix} \Delta \boldsymbol{\alpha}^a \\ \boldsymbol{\lambda} \end{bmatrix} \quad (43)$$

B. New ROE-Based Observability Criteria and Initial Costates for Optimal Evasive Maneuvers

To solve for the open-loop controller given in Eq. (42), the solution to $\boldsymbol{\lambda}(\tau)$ must be determined. This requires that the system dynamics represented by Eq. (43) to be solved, which ultimately needs $\boldsymbol{\lambda}(\tau_0)$. The solution to the linear time-varying system of Eq. (43) can be found using the following Peano–Baker formula for the linear time-varying state-transition matrix (see [40], pp. 106–117). Therefore, the solution to Eq. (43) is herein derived as

$$\dot{\boldsymbol{\Phi}}(\tau, \tau_0) = \begin{bmatrix} \boldsymbol{F}(\tau) & -\boldsymbol{B}(\tau) \boldsymbol{R}^{-1} \boldsymbol{B}^T(\tau) \\ \boldsymbol{0} & -\boldsymbol{F}(\tau)^T \end{bmatrix} \boldsymbol{\Phi}(\tau, \tau_0) \quad (44)$$

with $\boldsymbol{\Phi}(t_0, t_0) = \boldsymbol{I}$ denoting the initial state-transition matrix. The time-varying state-transition matrix can also be expressed as

$$\boldsymbol{\Phi}(\tau, \tau_0) = \begin{bmatrix} \boldsymbol{\Phi}_{\alpha^a}(\tau, \tau_0) & \boldsymbol{\Phi}_{\alpha^a \lambda}(\tau, \tau_0) \\ \boldsymbol{\Phi}_{\lambda \alpha^a}(\tau, \tau_0) & \boldsymbol{\Phi}_{\lambda}(\tau, \tau_0) \end{bmatrix} \quad (45)$$

Note that the matrix $\boldsymbol{B}(\tau)$ is also a time-varying function of the control input $\boldsymbol{u}$ due to the presence $\boldsymbol{B}''(\tau)$. However, at $\tau = 0$, the control inputs $\boldsymbol{u}$ is equal to $\boldsymbol{0}_3$. Therefore, the solution to the time-varying state-transition matrix can be initialized with $\boldsymbol{B}(\tau_0)$ using the first-order integral form of GVEs such that $\boldsymbol{B}''(\tau_0) = \boldsymbol{0}_{8\times 3}$.

The solution to Eq. (43) is therefore determined as

$$\begin{bmatrix} \Delta \boldsymbol{\alpha}^a(\tau) \\ \boldsymbol{\lambda}(\tau) \end{bmatrix} = \begin{bmatrix} \boldsymbol{\Phi}_{\alpha^a}(\tau, \tau_0) & \boldsymbol{\Phi}_{\alpha^a \lambda}(\tau, \tau_0) \\ \boldsymbol{\Phi}_{\lambda \alpha^a}(\tau, \tau_0) & \boldsymbol{\Phi}_{\lambda}(\tau, \tau_0) \end{bmatrix} \begin{bmatrix} \Delta \boldsymbol{\alpha}^a(\tau_0) \\ \boldsymbol{\lambda}(\tau_0) \end{bmatrix} \quad (46)$$

Solving this equation is only dependent on the pursuer's orbital elements and the initial states and costates, which will guarantee an optimal trajectory $\Delta \boldsymbol{\alpha}(\tau)$ that minimizes the cost function of Eq. (34). Solving for $\Delta \boldsymbol{\alpha}(\tau)$ and applying the ROE to LVLH conversion using Eq. (9) results in the relation for $\boldsymbol{\rho}(\tau)$,

$$\boldsymbol{\rho}(\tau) = \boldsymbol{\Phi}_{\mathrm{LVLH}}^a \Big[\boldsymbol{\Phi}_{\alpha^a} \Delta \alpha_0^a + \boldsymbol{\Phi}_{\alpha^a \lambda} \boldsymbol{\lambda}_0\Big] \quad (47)$$

which is the ROE equivalent to Eq. (4) such that

$$\boldsymbol{\Phi}_{\rho\rho} \boldsymbol{\rho}_0 + \boldsymbol{\Phi}_{\rho\dot{\rho}} \dot{\boldsymbol{\rho}}_0 + \int_{\tau_0}^{\tau} \boldsymbol{\Phi}_{\rho\dot{\rho}}(\tau, \mu) \boldsymbol{u}(\mu) \, \mathrm{d}\mu = \boldsymbol{\Phi}_{\mathrm{LVLH}}^a \Big[\boldsymbol{\Phi}_{\boldsymbol{\alpha}^a} \Delta \boldsymbol{\alpha}_0^a + \boldsymbol{\Phi}_{\alpha^a \lambda} \boldsymbol{\lambda}_0\Big] \quad (48)$$

The measurement profile based on ROE can herein be derived by substituting Eq. (47) into Eq. (6), that is,

$$\boldsymbol{i}_m(\tau) = \frac{\boldsymbol{\Phi}_{\mathrm{LVLH}}^a [\boldsymbol{\Phi}_{\alpha^a} \Delta \boldsymbol{\alpha}_0^a + \boldsymbol{\Phi}_{\alpha^a \lambda} \boldsymbol{\lambda}_0]}{||\boldsymbol{\Phi}_{\mathrm{LVLH}}^a [\boldsymbol{\Phi}_{\alpha^a} \Delta \boldsymbol{\alpha}_0^a + \boldsymbol{\Phi}_{\alpha^a \lambda} \boldsymbol{\lambda}_0]||} \quad (49)$$

Similar to the observability criteria defined by Woffinden and Geller [2], if the control acceleration is applied along the LOS vector such that

$$\boldsymbol{\Phi}_{\mathrm{LVLH}}^a \boldsymbol{\Phi}_{\alpha^a \lambda} \boldsymbol{\lambda}_0 = \eta(\tau) \boldsymbol{\Phi}_{\mathrm{LVLH}}^a \boldsymbol{\Phi}_{\alpha^a} \Delta \boldsymbol{\alpha}_0^a \quad (50)$$

which substituting into Eq. (49) results in

$$\boldsymbol{i}_m(\tau) = \frac{\boldsymbol{\Phi}_{\mathrm{LVLH}}^a [\boldsymbol{\Phi}_{\alpha^a} \Delta \boldsymbol{\alpha}_0^a + \eta(\tau) \boldsymbol{\Phi}_{\alpha^a} \Delta \boldsymbol{\alpha}_0^a]}{||\boldsymbol{\Phi}_{\mathrm{LVLH}}^a [\boldsymbol{\Phi}_{\alpha^a} \Delta \boldsymbol{\alpha}_0^a + \eta(\tau) \boldsymbol{\Phi}_{\alpha^a} \Delta \boldsymbol{\alpha}_0^a]||} = \frac{\boldsymbol{\Phi}_{\mathrm{LVLH}}^a ([1 + \eta(\tau)] \boldsymbol{\Phi}_{\alpha^a} \Delta \boldsymbol{\alpha}_0^a)}{||\boldsymbol{\Phi}_{\mathrm{LVLH}}^a ([1 + \eta(\tau)] \boldsymbol{\Phi}_{\alpha^a} \Delta \boldsymbol{\alpha}_0^a)||} \quad (51)$$

New observability criteria can now be inferred from the previous equations. Specifically, as with Woffinden and Geller's observability criteria, the angle-only navigation becomes unobservable when $\eta(\tau) > -1$. The ROE-based observability criteria are tabulated in Table 2.

For performing evasive maneuvers from a pursuer, the navigation system onboard the pursuer must be rendered unobservable through the previous condition by selecting $\eta(\tau) > -1$. For the purposes of this paper, the multiplication factor $\eta(\tau)$ can henceforth be denoted as the control coefficient. Based on the observability criteria and the fact that the transformation matrix $\boldsymbol{\Phi}_{\mathrm{LVLH}}^a$ appears on both sides of the

Table 2 New relative orbital elements observability criteria

Observable	$\boldsymbol{\Phi}^{a}_{\text{LVLH}}\boldsymbol{\Phi}_{\alpha^a\lambda}\boldsymbol{\lambda}_0 \neq \boldsymbol{\Phi}^{a}_{\text{LVLH}}[\eta(\tau)\boldsymbol{\Phi}_{\alpha^a}\Delta\boldsymbol{\alpha}^a_0]$	for any $\eta(\tau)$
Observable	$\boldsymbol{\Phi}^{a}_{\text{LVLH}}\boldsymbol{\Phi}_{\alpha^a\lambda}\boldsymbol{\lambda}_0 = \boldsymbol{\Phi}^{a}_{\text{LVLH}}[\eta(\tau)\boldsymbol{\Phi}_{\alpha^a}\Delta\boldsymbol{\alpha}^a_0]$	for $\eta(\tau) < -1$
Unobservable	$\boldsymbol{\Phi}^{a}_{\text{LVLH}}\boldsymbol{\Phi}_{\alpha^a\lambda}\boldsymbol{\lambda}_0 = \boldsymbol{\Phi}^{a}_{\text{LVLH}}[\eta(\tau)\boldsymbol{\Phi}_{\alpha^a}\Delta\boldsymbol{\alpha}^a_0]$	for $\eta(\tau) > -1$

equations in Table 2 defining the conditions, the initial costate can be determined through the equation

$$\boldsymbol{\lambda}_0 = \boldsymbol{\Phi}^{-1}_{\alpha^a\lambda}\left[\eta(\tau)\boldsymbol{\Phi}_{\alpha^a}\Delta\boldsymbol{\alpha}^a_0\right] \tag{52}$$

which results in an optimal evasive trajectory calculated using Eq. (46) that guarantees unobservability in the estimation of relative trajectories.

Because of the formulation of the dynamical model which includes SRP and a drag ballistic coefficient, both of which do not have a dynamical representation, the inverse $\boldsymbol{\Phi}^{-1}_{\alpha^a\lambda}(\tau,\tau_0)$ is singular. However, because the ballistic coefficients at the initial and final time are the same (i.e., they are assumed to be constant with time), the last two elements of the operation for $[\eta(\tau)\boldsymbol{\Phi}_{\alpha^a}\Delta\boldsymbol{\alpha}^a_0]$ are equal to the initial relative ballistic coefficients, that is,

$$\Delta B^{\text{SRP}}(\tau) = \Delta B^{\text{SRP}}(\tau_0) \qquad \Delta B^{\text{Drag}}(\tau) = \Delta B^{\text{Drag}}(\tau_0)$$

This means that they need not be included in determining the final two elements of $\boldsymbol{\lambda}(\tau_0)$, which are always zero as a result of the boundary conditions from optimal control theory. Therefore, the first six elements of $\boldsymbol{\lambda}(\tau_0)$ can be determined as

$$\boldsymbol{\lambda}_r(\tau_0) = \boldsymbol{\Phi}^{-1}_{\alpha^a\lambda_r}(\tau,\tau_0)\boldsymbol{e}_r \tag{53}$$

where the subscript r denotes the reduced matrix such that $\boldsymbol{\lambda}_r(\tau_0) \in \mathbb{R}^6$ and $\boldsymbol{\Phi}^{-1}_{\alpha^a\lambda_r}(\tau,\tau_0) \in \mathbb{R}^{6\times 6}$, which is found by determining the inverse of the first six rows and columns of $\boldsymbol{\Phi}_{\alpha^a\lambda}(\tau,\tau_0)$. The matrix $\boldsymbol{e}_r$ denotes the first six elements after the evaluation of the full equation represented by $[\eta(\tau)\boldsymbol{\Phi}_{\alpha^a}\Delta\boldsymbol{\alpha}^a_0]$, which allows the consideration of spacecraft ballistic coefficients when propagating the relative orbital elements in $\boldsymbol{\Phi}_{\alpha^a}(\tau,\tau_0)\Delta\boldsymbol{\alpha}^a(\tau_0)$.

C. Algorithm

This section presents the procedure, summarized in steps, of the optimal evasive maneuver implementation by using the equations presented in the previous sections:

1) For initialization, a set of osculating orbital elements are first initialized for the pursuer, $\boldsymbol{\alpha}^a{}_p(\tau_0) = [a_{p_0}, e_{p_0}, i_{p_0}, \omega_{pu_0}, \Omega_{p_0}, M_{p_0}, B^{\text{SRP}}_{p_0}, B^{\text{Drag}}_{p_0}]^T$. A set of osculating orbital elements for the evader is also initialized, $\boldsymbol{\alpha}^a{}_e(\tau_0) = [a_{e_0}, e_{e_0}, i_{e_0}, \omega_{e_0}, \Omega_{e_0}, M_{e_0}, B^{\text{SRP}}_{e_0}, B^{\text{Drag}}_{e_0}]^T$, such that the initial relative osculating orbital elements can be calculated as $\Delta\boldsymbol{\alpha}^a(\tau_0) = \boldsymbol{\alpha}^a_e(\tau_0) - \boldsymbol{\alpha}^a_p(\tau_0)$.

2) Select the variable $\eta(\tau)$ and the desired evasive time, $T_e = \Delta\tau = \tau_f - \tau_0$. The constant multiplication factor for the LOS vector $\eta(\tau)$ is selected depending on how much separation distance is desired between the evader and the pursuer RSO. The larger the value is, the larger the separation distance at the end of the maneuver is. Furthermore, the time of flight should be selected proportionally in order to avoid overshoots and reduce fuel consumption.

3) Propagate the linear time-varying state-transition matrix of Eq. (44), which can then be stored in memory, and calculate the initial costates using Eq. (52).

4) Using the linear time-varying state-transition matrix, the initial states from step 1, and costates from step 3, calculate the optimal trajectory from $\Delta\boldsymbol{\alpha}^a(\tau_0)$ to $\Delta\boldsymbol{\alpha}^a(\tau_f)$ using Eq. (46). The optimal relative trajectory in the LVLH frame can then be calculated with Eq. (18). The open-loop optimal control maneuvers $\boldsymbol{u}_\alpha$ for the evader can be calculated using Eq. (42).

IV. Simulation Results

This section presents the closed-loop simulations for the newly developed optimal evasive maneuvers. The pursuer spacecraft employs a two-point optimal guidance law developed by Chihabi and Ulrich [26] in combination with a Guardian map-based Simple Adaptive Control law [41]. Furthermore, the onboard relative navigation system employs an adaptive extended Kalman filter proposed by Fraser and Ulrich [42] modified to the angle-only measurement model and orbital elements-based process dynamics by Chihabi and Ulrich [43]. For all simulation cases, the Kalman filter was initialized with the following values: $\boldsymbol{P}_0 = (1\times 10^{-20})\boldsymbol{I}_6$, $\boldsymbol{Q}_0 = (1\times 10^{-14})\boldsymbol{I}_6$, $\boldsymbol{R}_0 = (1\times 10^{-4})\boldsymbol{I}_3$, and a white Gaussian noise standard deviation of 0.0032 deg for measurement angles α_m and β_m. The Kalman filter employs the same dynamics model used within the optimal guidance law developed by Chihabi and Ulrich and the optimal evasive maneuver development of this Note which contain the perturbing effects of J_2 luni-solar third-body, atmospheric drag and SRP.

The numerical propagator used as the truth model integrates the inertial two-body equation of motion to which the inertial perturbing accelerations are added. Specifically, perturbing accelerations due to gravitational field through the expansion of gravitational potential function up to degree and order 180; third-body effects of the sun, moon, solar system planets; ocean and solid Earth tidal effects; relativity; SRP; and drag are included. This numerical propagator is developed within the MATLAB®/Simulink environment using the International Astronomical Union's software package for dynamical astronomy, which features the most accurate numerical propagation of spacecraft and celestial bodies. In MATLAB®, an ODE45 solver with a relative and absolute tolerance of 1×10^{-9} was selected for all cases. This is thus slightly different than the dynamics model used in the optimization problem. As a result, these modeling mismatches would negatively impact the (lack of) observability.

The initial time was selected as 1 July 2014 for planetary ephemeris. The mass and cross-sectional area are 211 kg and 1.77 m^2 and 339 kg and 3.34 m^2 for the chaser and target spacecraft, respectively. For the solar radiation pressure model, a constant coefficient of reflectivity of 2 is used for both spacecraft. No maneuver execution errors are modeled for both spacecraft.

A. Low Earth Orbit

The osculating orbital elements for low Earth orbit (LEO) are selected as $a_p = 7947$ km, $e_p = 0.1343248$, $i_p = 79.7965$ deg, $\omega_p = 165.8128$ deg, $\Omega_p = 261.0864$ deg, and $\theta_p = 194.2893$ deg. The initial orbital elements for the evader were selected such that $\Delta\boldsymbol{\alpha}(\tau_0) = [-0.5\ \ -5\times 10^{-4}\ \ -1\text{ deg}\ \ -1\text{ deg}\ \ 1\text{ deg}\ \ -0.2\text{ deg}]^T$. The duration of the simulation corresponding to the pursuer's rendezvous time was selected as 5000 s.

Figure 3 shows the relative motion in the evader's LVLH reference frame in which the red dashed line represents the pursuer's desired path, and Fig. 4 shows the relative navigation errors, both without evasive maneuvers applied. Figures 5 and 6 show the same except with evasive maneuvers with $\eta(\tau) = 0.5$ and evasive time of $T_e = 1000$ s. When comparing the results, it is clear that the optimal evasive algorithm indeed does result in unobservable measurements in the pursuer's navigation system because the navigation errors diverge, as shown in Fig. 6. Furthermore, Fig. 7 shows the control accelerations remain low on the order of 10^{-3} m/s^2, resulting in a total Delta-V requirement of approximately 11 m/s.

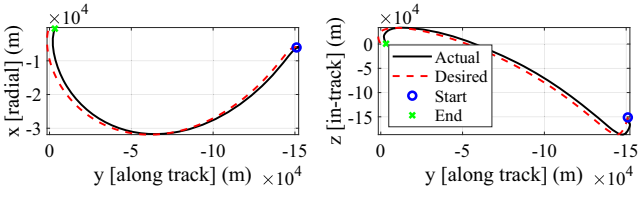

Fig. 3 LEO scenario pursuer path in LVLH without evasive maneuvers.

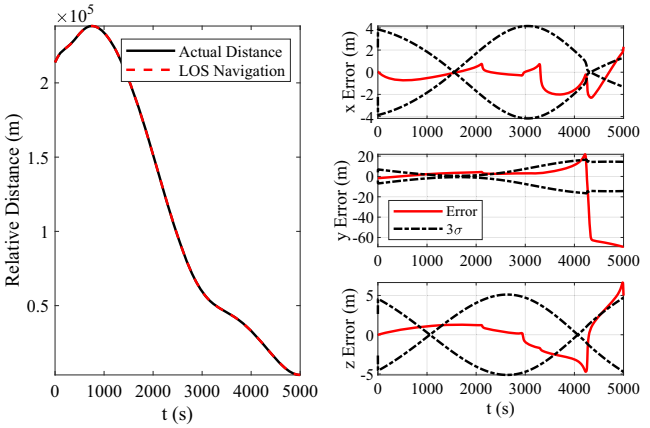

Fig. 4 LEO scenario pursuer relative navigation errors without evasive maneuvers.

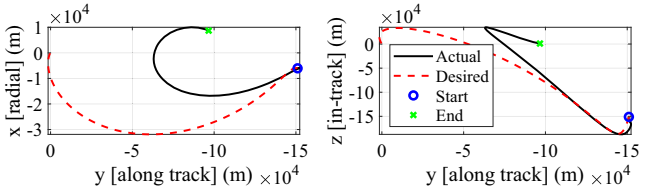

Fig. 5 LEO scenario pursuer path in LVLH with evasive maneuvers.

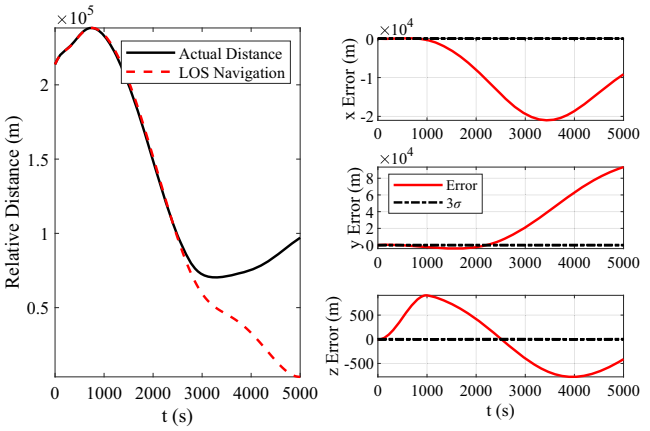

Fig. 6 LEO scenario pursuer relative navigation errors with evasive maneuvers.

For the same LEO initial conditions, a sensitivity analysis is performed by varying $\eta(\tau)$ and T_e to observe the effects on Delta-V requirement, maximum distance between the evader and pursuer, and navigation error at the end of the scenario. The results are provided in Fig. 8, in which the error is calculated as $\sqrt{(x_{\text{true}} - x_{\text{nav}})^2 + (y_{\text{true}} - y_{\text{nav}})^2 + (z_{\text{true}} - z_{\text{nav}})^2}$.

When observing the results, it can be seen that applying $\eta(\tau) = 0$ results in a Delta-V requirement of 0 m/s. This is due to the fact that the evasive maneuver time derivative of the costates only varies as a function of the costates themselves and selecting $\eta(\tau) = 0$ results in $\mathbf{0}$ for the initial costates, therefore yielding no control actuation based on Eq. (42). Furthermore, as the evasive maneuver time is decreased, the slope of the curves become steeper, implying larger control efforts with larger maximum distance and errors at the end of the scenario. This also true when varying the value for $\eta(\tau)$, which is expected because the optimal evasive law represented by Eq. (50) represents a desired maximum distance between the spacecraft at the end of the maneuver and hence larger control demand.

B. Highly Elliptical Orbit

The initial osculating orbital elements for the highly elliptical orbit example were initialized as $a_p = 40000$ km, $e_p = 0.8325$, $i_p = 90.0$ deg, $\omega_p = 350$ deg, $\Omega_p = 100.0$ deg, and $\theta_p = 100$ deg. The initial ROE $\Delta\boldsymbol{\alpha}(\tau_0)$ is equivalent to the one selected for the LEO case with the same scenario duration. The highly elliptical orbit (HEO) scenario shown by Figs. 9–13 aims to evaluate and compare the performance of the evasive maneuver formulation by keeping all the conditions the same between the HEO and LEO scenarios and only changing the orbital regime.

Figures 9 and 10 show the relative motion in the evader's LVLH reference frame and relative navigation errors, respectively, without evasive maneuvers. Figures 11 and 12 shows the same except with evasive maneuvers with $\eta(\tau) = 0.5$ and evasive time of $T_e = 1000$ s. When comparing the results, the optimal evasive algorithm results in unobservable measurements in the pursuer's navigation system, and hence the algorithm remains applicable to highly elliptical orbit scenarios, thanks to the use of the ROE dynamical model. Furthermore, Fig. 13 shows the control accelerations remain on below 1 m/s^2, resulting in a total Delta-V requirement of approximately 963 m/s with a maximum separation distance between the spacecraft of approximately 3500 km at the end of the maneuver. This high Delta-V requirement is due to the fact the reference orbit is that of a highly elliptical one, resulting in larger maximum distance and hence larger control demand when compared to the LEO scenario while using the same values for $\eta(\tau)$ and evasive time T_e.

A sensitivity analysis is also performed for the HEO scenario by varying $\eta(\tau)$ and T_e to observe the effects on Delta-V requirement, maximum distance between the evader and pursuer, and navigation error at the end of the scenario. The results are plotted and shown in Fig. 14. Similarly to the LEO scenario, as the evasive maneuver time is decreased, the slopes of the curves become steeper, resulting in larger control efforts with larger maximum distance and errors at the end of the scenario. There is a slight asymmetry observed in Fig. 14 for the same positive and negative values of $\eta(\tau)$. The negative value of $\eta(\tau)$ implies a maneuver that is opposite of the line-of-sight vector (i.e., toward the pursuer spacecraft), so slight asymmetry is expected for such a maneuver. Because a Delta-V of 963 m/s is not ideal, the results shown in Fig. 14 demonstrate other options that are available to reduce the Delta-V by tuning the evasive maneuver time and control coefficient.

Table 3 shows the maximum errors, distances, evasive maneuver times, and control coefficients, corresponding to picking a low Delta-V from Fig. 14, of 10 m/s. It can be seen that a maximum

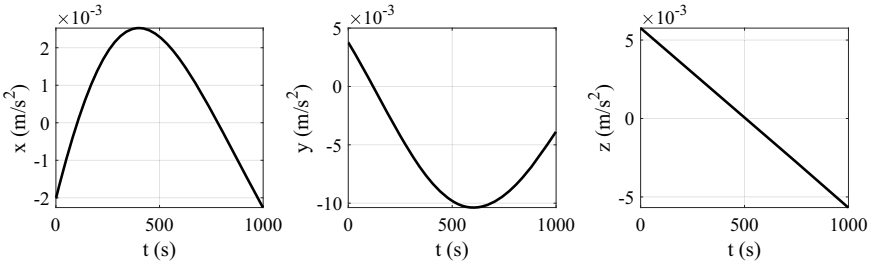

Fig. 7 LEO evader control for $T_e = 1000$ s and $\eta(\tau) = 0.5$.

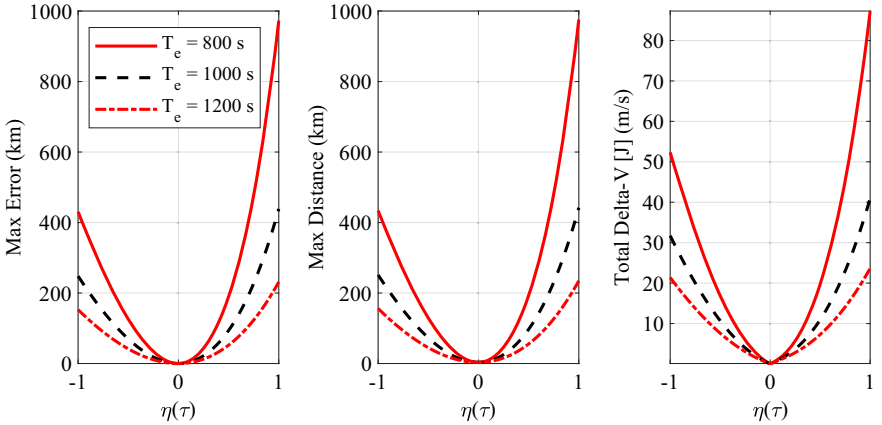

Fig. 8 LEO scenario comparison of $\eta(\tau)$ values and evasive maneuver time T_e.

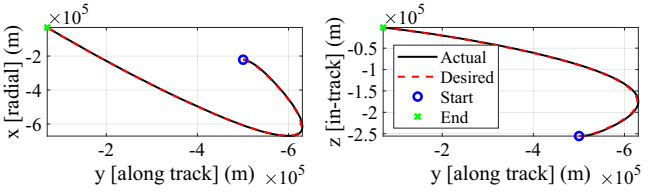

Fig. 9 HEO scenario pursuer path in LVLH without evasive maneuvers.

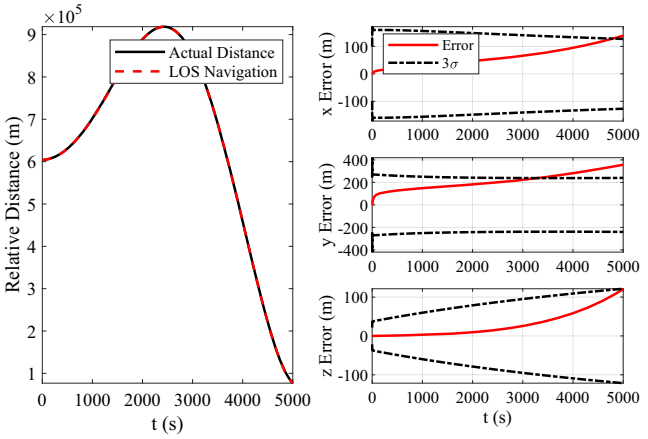

Fig. 10 HEO scenario pursuer relative navigation errors without evasive maneuvers.

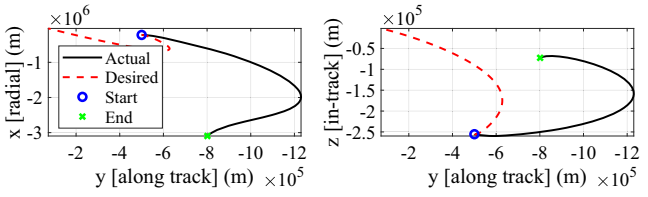

Fig. 11 HEO scenario pursuer path in LVLH with evasive maneuvers.

navigation error of 29.2693 km occurs at a value of $\eta(\tau) = -0.1717$ and $T_e = 2000$, while a maximum distance of 98.2246 km at the end of the scenario occurs when $\eta(\tau) = 0.2727$ and $T_e = 2500$. Comparing these values with the trends in Fig. 14, it is evident that a shorter-duration evasive maneuver time correlates with a larger maximization of navigation error at the end of the scenario while increasing the control coefficient $\eta(\tau)$ increases the maximum distance at the end of the scenario.

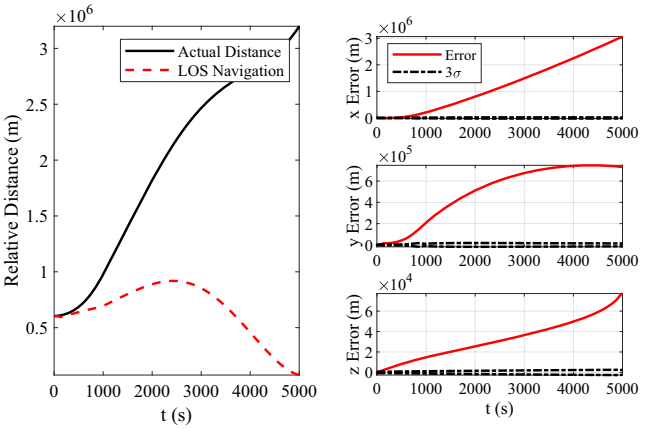

Fig. 12 HEO scenario pursuer relative navigation errors with evasive maneuvers.

V. Conclusions

This work presented a simple, yet effective, methodology for optimal evasive maneuvers using relative orbital elements in a perturbed pursuer–evader scenario. Specifically, the guidance and control law builds upon previous work in the areas of observability of angle-only measurements for circular reference orbits, optimal control theory, and relative orbital elements dynamical modeling. The dynamical model used in this formulation contains the effects of gravitational, third-body, atmospheric drag, and solar radiation pressure augmented with the second-order Gauss variational equations to consider control inputs. This new formulation resulted in novel relative orbital elements-based observability criteria that is applicable to perturbed highly elliptical orbits and arbitrary separation distances. The application of nonlinear optimal control theory to the new observability criteria and dynamical formulation allowed for the design of necessary evasive maneuvers to maximize the final separation distance while rendering the pursuer's onboard angle-only navigation system unobservable.

Two pursuer–evader scenarios, one on a highly elliptical reference orbit and the other in low Earth orbit, were simulated. The results demonstrated the effectiveness of the proposed guidance and control law in successfully rendering the pursuer's onboard relative navigation system unobservable, thereby resulting in successful evasive maneuvers. Furthermore, a sensitivity analysis was performed by varying evasive maneuver time and the constant scaling factor for the line-of-sight vector. The analysis showed that as the maneuver time increases the required Delta-V decreases. Similarly, it was shown that the maximum estimation error, the distance achieved at the end of the maneuver, and the required Delta-V were all directly proportional to the line-of-sight scaling factor. Future work will focus on reformulating the evasive maneuvers using a nonsingular orbital to

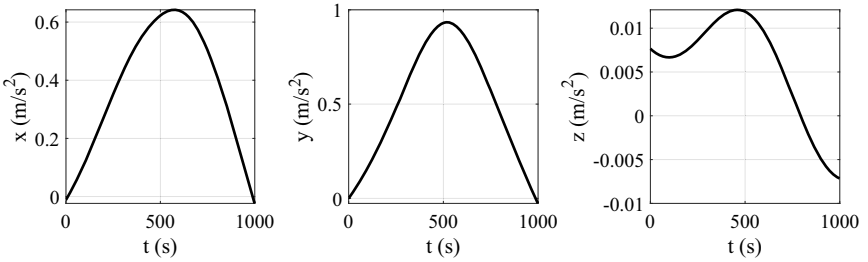

Fig. 13 HEO evader control for $T_e = 1000$ s and $\eta(\tau) = 0.5$.

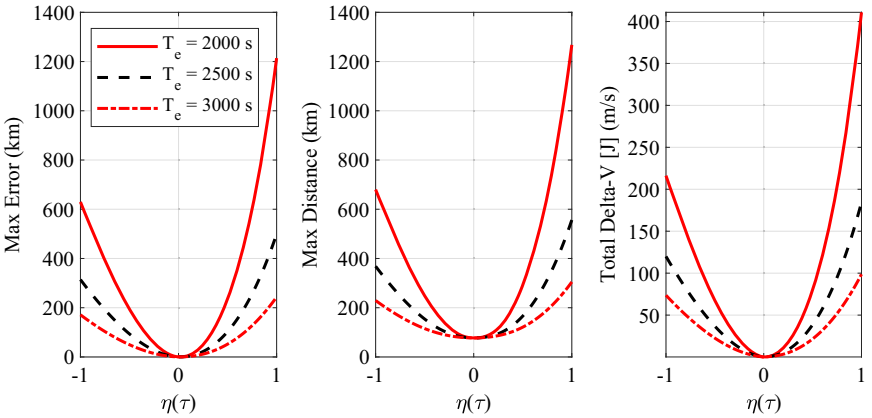

Fig. 14 HEO scenario comparison of $\eta(\tau)$ values and evasive maneuver time (T_e).

Table 3 Max error, distance, T_e, and $\eta(\tau)$ values for 10 m/s Delta-V

T_e, s	$\eta(\tau)$	Max error, km	Max distance, km
2000	−0.1717	29.2693	97.1306
2000	0.1919	27.1388	97.6276
2500	−0.2323	23.7590	93.2864
2500	0.2727	26.7160	98.2246
3000	−0.3131	21.3903	91.6771
3000	0.3535	24.4549	97.1695

accommodate for equatorial and circular orbits and formulating an efficient way to determine the evasive maneuver times and control coefficient in real time. The algorithm will also be expanded to include rendezvous detection and simulated for longer evasive maneuver times with lower thrust demand.

References

[1] Bevilacqua, R., Kumar, M., Alfriend, T., Krag, H., and Anselmo, L., "Special Issue on Space Situational Awareness from the 1st International Academy of Astronautics Conference on Space Situational Awareness or ICSSA 2017," *Acta Astronautica*, Vol. 155, Feb. 2019, pp. 367–368. https://doi.org/10.1016/j.actaastro.2019.02.027

[2] Woffinden, D., and Geller, D., "Observability Criteria for Angles-Only Navigation," *IEEE Aerospace and Electronic Systems Magazine*, Vol. 45, No. 3, 2009, pp. 1194–1208. https://doi.org/10.1109/TAES.2009.5259193

[3] Gaias, G., D'Amico, S., and Ardaens, J.-S., "Angles-Only Navigation to a Noncooperative Satellite Using Relative Orbital Elements," *Journal of Guidance, Control, and Dynamics*, Vol. 37, No. 2, 2014, pp. 439–451. https://doi.org/10.2514/1.61494

[4] Gaias, G., and Ardaens, J.-S., "Flight Demonstration of Autonomous Noncooperative Rendezvous in Low Earth Orbit," *Journal of Guidance, Control, and Dynamics*, Vol. 41, No. 6, 2018, pp. 1337–1354. https://doi.org/10.2514/1.G003239

[5] Isaacs, R., *Differential Games*, Wiley, New York, 1965, pp. 1–24.

[6] Sánchez-Ortiz, N., Belló-Mora, M., and Klinkrad, H., "Collision Avoidance Manoeuvres During Spacecraft Mission Lifetime: Risk Reduction and Required ΔV," *Advances in Space Research*, Vol. 38, No. 9, 2006, pp. 2107–2116. https://doi.org/10.1016/j.asr.2005.07.054

[7] Chan, K., "Spacecraft Maneuvers to Mitigate Potential Collision Threats," *AIAA/AAS Astrodynamics Specialist Conference*, AIAA Paper 2002-4629, 2002.

[8] Kim, H.-D., and Kim, H.-J., "Optimal Collision Avoidance Maneuver to Maintain a LEO Station Keeping," *61st International Astronautical Congress*, International Astronautical Congress, Prague, Czech Republic, IAC-10.A6.2.9, 2010, pp. 3056–3060.

[9] Kelly, B. D., and Picciotto, S. D., "Probability Based Optimal Collision Avoidance Maneuvers," *Space 2005*, AIAA Paper 2005-6775, 2005.

[10] Patera, R. P., "General Method for Calculating Satellite Collision Probability," *Journal of Guidance, Control, and Dynamics*, Vol. 24, No. 4, 2001, pp. 716–722. https://doi.org/10.2514/2.4771

[11] Patera, R. P., "Satellite Collision Probability for Nonlinear Relative Motion," *Journal of Guidance, Control, and Dynamics*, Vol. 26, No. 5, 2003, pp. 728–733. https://doi.org/10.2514/2.5127

[12] Patera, R. P., and Peterson, G. E., "Space Vehicle Maneuver Method to Lower Collision Risk to an Acceptable Level," *Journal of Guidance, Control, and Dynamics*, Vol. 26, No. 2, 2003, pp. 233–237. https://doi.org/10.2514/2.5063

[13] Bombardelli, C., "Analytical Formulation of Impulsive Collision Avoidance Dynamics," *Celestial Mechanics and Dynamical Astronomy*, Vol. 118, No. 2, 2014, pp. 99–114. https://doi.org/10.1007/s10569-013-9526-3

[14] Lee, S.-C., Kim, H. D., and Suk, J., "Collision Avoidance Maneuver Planning Using GA for LEO and GEO Satellite Maintained in Keeping Area," *International Journal of Aeronautical and Space Sciences*, Vol. 13, No. 4, 2012, pp. 474–483. https://doi.org/10.5139/IJASS.2012.13.4.474

[15] Kim, E. H., Kim, H. D., and Kim, H. J., Optimal Solution of Collision Avoidance Maneuver with Multiple Space Debris," *Journal of Space Operations*, Vol. 9, No. 3, 2012, pp. 20–31.

[16] de Jesus, A. D., and de Sousa, R. R., "Processing Optimized for Symmetry in the Problem of Evasive Maneuvers," *Computational and Applied Mathematics*, Vol. 34, No. 2, 2015, pp. 521–534. https://doi.org/10.1007/s40314-014-0147-6

[17] Wong, R. E., "Some Aerospace Differential Games," *Journal of Spacecraft and Rockets*, Vol. 4, No. 11, 1967, pp. 1460–1465. https://doi.org/10.2514/3.29114

[18] Anderson, G. M., "Feedback Control for a Pursuing Spacecraft Using Differential Dynamic Programming," *AIAA Journal*, Vol. 15, No. 8,

1977, pp. 1084–1088.
https://doi.org/10.2514/3.60758
[19] Burk, R. C., and Widhalm, J. W., "Minimum Impulse Orbital Evasive Maneuvers," *Journal of Guidance, Control, and Dynamics*, Vol. 12, No. 1, 1989, pp. 121–123.
https://doi.org/10.2514/3.20378
[20] Wang, Z., Gong, B., Yuan, Y., and Ding, X., "Incomplete Information Pursuit-Evasion Game Control for a Space Non-Cooperative Target," *Aerospace*, Vol. 8, No. 8, 2021, p. 211.
https://doi.org/10.3390/aerospace8080211
[21] Yu, D., Wang, H., Guo, S., and Wang, H., "Analytical Approach for Orbital Evasion with Space Geometry Considered," *International Journal of Aerospace Engineering*, Vol. 2017, March 2017, Paper 4164260.
[22] Clohessy, W. H., and Wiltshire, R. S., "Terminal Guidance System for Satellite Rendezvous," *Journal of the Aerospace Sciences*, Vol. 27, No. 9, 1960, pp. 653–658.
https://doi.org/10.2514/8.8704
[23] Chihabi, Y., and Ulrich, S., "Spacecraft Formation Guidance Law Using a State Transition Matrix with Gravitational, Drag and Third-Body Perturbations," *30th AIAA/AAS Space Flight Mechanics Meeting*, AIAA Paper 2020-1460, Jan. 2020.
[24] Chihabi, Y., and Ulrich, S., "Perturbed State-Transition Matrix for Spacecraft Formation Flying Terminal-Point Guidance," *Journal of Astronautical Sciences*, Vol. 68, No. 3, 2021, pp. 642–676.
https://doi.org/10.1007/s40295-021-00272-1
[25] Chihabi, Y., and Ulrich, S., "Linear Time-Varying State Transition Matrix for Spacecraft Relative Dynamics on Highly Elliptical Orbits," *Acta Astronautica*, Vol. 198, Sept. 2022, pp. 208–224.
https://doi.org/10.1016/j.actaastro.2022.05.056
[26] Chihabi, Y., and Ulrich, S., "Development and Experimental Validation of Two-Point Optimal Guidance for Spacecraft Formations," *AAS/AIAA Astrodynamics Specialist Conference*, American Astronomical Soc. Paper 21-500, Washington, D.C., 2021.
[27] Chihabi, Y., and Ulrich, S., "Software-in-the-Loop Validation of a Novel Two-Point Optimal Guidance for Perturbed Spacecraft Rendezvous and Formations," *Journal of Astronautical Sciences*, Vol. 70, No. 43, 2023, pp. 2195–0571.
https://doi.org/10.1007/s40295-023-00405-8
[28] Hammel, S. E., and Aidala, V. J., "Observability Requirements for Three-Dimensional Tracking via Angle Measurements," *IEEE Aerospace and Electronic Systems Magazine*, Vol. 2, March 1985, pp. 200–207.
https://doi.org/10.1109/TAES.1985.310617
[29] Nardone, S. C., and Aidala, V. J., "Observability Criteria for Bearings-Only Target Motion Analysis," *IEEE Aerospace and Electronic Systems Magazine*, Vol. 2, March 1981, pp. 162–166.
https://doi.org/10.1109/TAES.1981.309141
[30] Vallado, D. A., "Evaluating Gooding Angles-Only Orbit Determination of Space Based Space Surveillance Measurements," *US/Russian Workshop*, Paper USR 10-S4.5, 2010.
[31] Woffinden, D., and Geller, D., "Observability Criteria for Angles-Only Navigation," *IEEE Aerospace and Electronic Systems Magazine*, Vol. 45, No. 3, 2009, pp. 1194–1208.
https://doi.org/10.1109/TAES.2009.5259193
[32] Grzymisch, J., and Fichter, W., "Observability Criteria and Unobservable Maneuvers for In-Orbit Bearings-Only Navigation," *Journal of Guidance, Control, and Dynamics*, Vol. 37, No. 4, 2014, pp. 1250–1259.
https://doi.org/10.2514/1.62476
[33] Grzymisch, J., and Fichter, W., "Analytic Optimal Observability Maneuvers for In-Orbit Bearings-Only Rendezvous," *Journal of Guidance, Control, and Dynamics*, Vol. 37, No. 5, 2014, pp. 1658–1664.
https://doi.org/10.2514/1.G000612
[34] Lewis, F. L., *Applied Optimal Control & Estimation: Digitial Design & Implementation*, 1st ed., Prentice–Hall, Upper Saddle River, NJ, 1992, pp. 120–124.
[35] Gurfil, P., and Kholshevnikov, K. V., "Manifolds and Metrics in the Relative Spacecraft Motion Problem," *Journal of Guidance, Control, and Dynamics*, Vol. 29, No. 4, 2006, pp. 1004–1010.
https://doi.org/10.2514/1.15531
[36] Gurfil, P., and Kholshevnikov, K. V., "Distances on the Relative Spacecraft Motion Manifold," *AIAA Guidance, Navigation and Control Conference and Exhibit*, AIAA Paper 2005-5859, 2005.
[37] Schaub, H., and Junkins, J. L., *Analytical Mechanics of Space Systems*, AIAA, Reston, VA, 2018, pp. 593–673.
[38] Chihabi, Y., and Ulrich, S., "Analytical Spacecraft Relative Dynamics with Gravitational, Drag and Third-Body Perturbations," *Acta Astronautica*, Vol. 185, Aug. 2021, pp. 42–57.
https://doi.org/10.1016/j.actaastro.2021.04.043
[39] Zhang, G., and Mortari, D., "Second-Order Integral-Form Gauss's Variational Equations Under Impulsive Control," *Journal of Guidance, Control, and Dynamics*, Vol. 42, No. 2, 2019, pp. 284–302.
https://doi.org/10.2514/1.G003607
[40] Chen, C.-T., *Linear System Theory and Design*, Saunders College Publ., Philadelphia, PA, 1999, pp. 106–117.
[41] Chihabi, Y., and Ulrich, S., "Hybrid Guardian Map-Based Adaptive Control of Spacecraft Formation Flying on Highly Elliptical Orbits in the Restricted Three-Body Problem," *Acta Astronautica*, Vol. 180, March 2021, pp. 370–385.
https://doi.org/10.1016/j.actaastro.2020.12.048
[42] Fraser, C. T., and Ulrich, S., "Adaptive Extended Kalman Filtering Strategies for Spacecraft Formation Relative Navigation," *Acta Astronautica*, Vol. 178, Jan. 2021, pp. 700–721.
https://doi.org/10.1016/j.actaastro.2020.10.016
[43] Chihabi, Y., and Ulrich, S., "Nonlinear Adaptive Angle-Only Relative Navigation on Perturbed Eccentric Orbits," *33rd AAS/AIAA Space Flight Mechanics Meeting*, American Astronomical Soc. Paper 23-111, Washington, D.C., Jan. 2023.